Proteolytic activation of SARS-CoV-2 spike at the S1/S2 boundary: potential role of proteases beyond furin

Tiffany Tang[1], Javier A. Jaimes[2], Miya K. Bidon[1], Marco R. Straus[2], Susan Daniel[1*], Gary R. Whittaker[2*]

[1]Robert Frederick Smith School of Chemical and Biomolecular Engineering, Cornell University, Ithaca, NY, 14853, USA

[2]Department of Microbiology and Immunology, Cornell University, Ithaca, NY, 14853, USA

*Corresponding authors:

Gary Whittaker: grw7@cornell.edu

Susan Daniel: sd386@cornell.edu

Abstract

The severe acute respiratory syndrome coronavirus 2 (SARS-CoV-2) uses its spike (S) protein to mediate viral entry into host cells. Cleavage of the S protein at the S1/S2 and/or S2' site(s) is associated with viral entry, which can occur at either the cell plasma membrane (early pathway) or the endosomal membrane (late pathway), depending on the cell type. Previous studies show that SARS-CoV-2 has a unique insert at the S1/S2 site that can be cleaved by furin, which appears to expand viral tropism to cells with suitable protease and receptor expression. Here, we utilize viral pseudoparticles and protease inhibitors to study the impact of the S1/S2 cleavage on infectivity. Our results demonstrate that S1/S2 pre-cleavage is essential for early pathway entry into Calu-3 cells, a model lung epithelial cell line, but not for late pathway entry into Vero E6 cells, a model cell line. The S1/S2 cleavage was found to be processed by other proteases beyond furin. Using bioinformatic tools, we also analyze the presence of a furin S1/S2 site in related CoVs and offer thoughts on the origin of the insertion of the furin-like cleavage site in SARS-CoV-2.

Keywords: SARS-CoV-2, furin, S1/S2 site, viral entry, cleavage

29 **Introduction**

30 The 21st century has seen the rise of pathogenic strains of human coronaviruses (CoVs) causing major
31 public health concerns, first with the severe acute respiratory syndrome coronavirus (SARS-CoV) in 2002[1],
32 then with Middle East respiratory syndrome coronavirus (MERS-CoV) in 2012[2], and now, with the severe
33 acute respiratory syndrome coronavirus 2 (SARS-CoV-2). SARS-CoV-2 causes the disease syndrome known
34 as COVID-19[3], now classified as a pandemic with global reach and impact.

35 CoV host cell entry is mediated by its spike (S) glycoprotein, a large transmembrane protein that decorates
36 the virus particle[4]. The S protein is demarcated into two domains, the S1 and S2 domain, which contains
37 the receptor binding domain and membrane fusion domain, respectively. There are two proteolytic
38 activation events associated with S-mediated membrane fusion[5]. The first is a priming cleavage that
39 occurs at the interface of the S1 and S2 domain (S1/S2) for some coronaviruses, and the second is the
40 obligatory triggering cleavage that occurs within the S2 region (S2')[5]. The priming cleavage generally
41 converts the S protein into a fusion competent form, by enabling the S protein to better bind receptors or
42 expose hidden cleavage sites[5]. The triggering cleavage initiates a series of conformational changes that
43 enable the S protein to harpoon into the host membrane for membrane fusion[5].

44 There are a variety of proteases capable of priming and triggering CoV S proteins. While the priming event
45 is not as well characterized and virus dependent, it has been observed that the CoV S can be triggered by
46 proteases at the plasma membrane or endosomal membrane, enabling entry in what are termed "early"
47 and "late" pathways, respectively[6–8]. SARS-CoV was found to utilize the transmembrane bound protease
48 TMPRSS2 to enter using the early pathway[8–10]. However, TMPRSS2 expression is limited to epithelial cell
49 lines, and in TMPRSS2 negative cell lines, SARS-CoV utilizes endosomal cathepsin L to enter using the late
50 pathway[11]. MERS-CoV also utilizes TMPRSS2 and cathepsin L with one major difference. The MERS-CoV
51 S1/S2 boundary contains an RSVR insert that can be recognized by furin or related proprotein convertases

52 (PC), proteases commonly found in the secretory pathway of most cell lines[7,12]. During the S maturation
53 process, the S protein can be cleaved by furin/PCs[7,12]. Thus, MERS-CoV particles harbor cleaved S1/S2
54 protein and it was observed that the S1/S2 priming (pre-cleavage) is crucial for MERS-CoV[7], but not SARS-
55 CoV[13], to infect via the early pathway route. However, the S1/S2 cleavage is not a requirement for MERS-
56 CoV late pathway infection[7].

57 For SARS-CoV-2, early studies showed that the S1/S2 junction contains an insert with two additional basic
58 residues, P-R-R-A (P – proline, R – arginine, A – alanine), that was not present in SARS-CoV or its closest
59 bat ancestor viruses[14,15]. This insert forms a P-R-R-A-R sequence and while it does contain the minimum
60 furin recognition motif, R-X-X-R, it diverges from the preferred R-X-K/R-R motif, because the SARS-CoV-2
61 sequence has an A in the P3 location instead of an R[16,17] (**Figure 1**). Intriguingly, the only other known
62 example of this insert on FurinDB[18], a database of furin substrates, is found in proaerolysin, a bacterial
63 toxin, and was determined to be activated by furin[19].

64 Indeed, early studies suggest that SARS-CoV-2 is also processed by furin since SARS-CoV-2 harbors a
65 cleaved S protein, likely due to furin processing at the S1/S2 site[20–22]. Similar to what was observed for
66 MERS-CoV, this S1/S2 cleavage was determined to be a prerequisite for subsequent TMPRSS2 activation
67 at the S2' site for infection of respiratory cell lines, such as Calu-3[23,24]. Furthermore, like MERS-CoV, SARS-
68 CoV-2 can also utilize cathepsin L in the endosomal pathway in TMPRSS2-negative cell lines, such as Vero
69 E6[22].

70 In this study, we sought to better characterize the SARS-CoV-2 S1/S2 cleavage site and raise some
71 intriguing possibilities for how the site might have emerged. Using pseudoparticles and protease inhibitors,
72 we investigated the impact of S1/S2 cleavage for successful infection of cells via the early and late pathway.
73 Our data shows that the S1/S2 cleavage is essential for subsequent S2' activation via TMPRSS2 for entry

74 in Calu-3 cells, but not for S2' activation via cathepsin L for entry in Vero E6 cells, and suggests that furin

75 may not be the only protease responsible for the S1/S2 cleavage event.

76

77 **Figure 1**

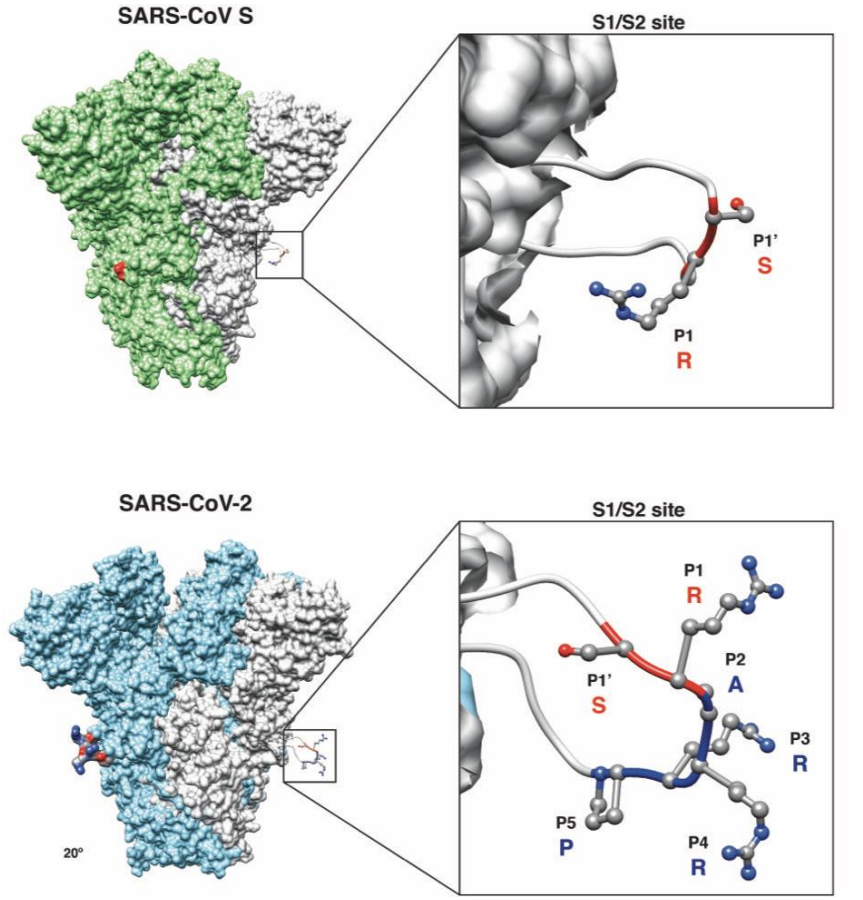

78

79 **Figure 1**: Predicted structural model of the SARS-CoV and SARS-CoV-2 S proteins. (**Inset**) Magnification of
80 the S1/S2 site with conserved R and S residues (red ribbon) and the unique four amino acid insertion P-R-
81 R-A for SARS-CoV-2 (blue ribbon) are shown. The P's denote the position of that amino acid from the S1/S2
82 cleavage site, with P1-P5 referring to amino acids before the cleavage site and P1' referring to amino acids
83 after the cleavage site.

84 **Results and Discussion**

85 **MLV pseudoparticles as a system to study SARS-CoV-2 entry**. To assess the functional importance of the
86 S1/S2 site for SARS-CoV-2 entry, we utilized viral pseudoparticles. These particles consist of a murine
87 leukemia virus (MLV) core and are decorated with the viral envelope protein to accurately recapitulate
88 the entry steps of their native counterpart[25]. These particles also contain a luciferase reporter that
89 integrates into the host cell genome upon successful infection and drives the cells to produce luciferase,
90 which is quantifiable. We and others have used MLV-based pseudoparticles widely to study CoV entry
91 pathways[12,21,26]. Using the HEK293T cell line, MLV pseudoparticles containing the wild type SARS-CoV-2 S
92 protein (SARS-CoV-2pp), or the SARS-CoV S protein (SARS-CoVpp) were generated alongside positive
93 control particles containing the vesicular stomatitis virus G protein (VSVpp) or negative control particles
94 lacking envelope proteins (Δenvpp).

95 Since coronaviruses can enter via the ”early” or “late” pathway, we chose to infect cell lines representative
96 of each pathway, as the entry mechanism can be highly cell-type dependent[27]. We utilized the Calu-3
97 (early) and the Vero E6 (late) cell lines for these studies, which activate the SARS-CoV-2 S2’ using TMPRSS2
98 and cathepsin L, respectively. As expected, VSVpp (positive control) infected Vero E6 and Calu-3 cells with
99 several orders of magnitude higher luciferase units than the values reported with Δenvpp infection
100 (negative control) (**Figure 2A, 2B**). This confirms that the envelope protein is driving infection, and not the
101 particle itself. In the case of SARS-CoVpp and SARS-CoV-2pp, both particles are infectious in both cell lines
102 as they drive luciferase production several orders of magnitude higher than Δenvpp. (**Figure 2A, 2B**), with
103 SARS-CoVpp more infectious than SARS-CoV-2pp.

104 The pseudoparticles were also probed for their S content via western blot. For the SARS-CoV-2pp, we
105 detected a band at 85 kDa and for SARS-CoVpp, a strong band at 185 kDa (**Figure 2C**)**.** The different bands
106 observed between SARS-CoV-2pp and SARS-CoVpp is likely because SARS-CoV-2 S is cleaved at the S1/S2

107 location by furin/PCs during biosynthesis, while SARS-CoV S cannot be cleaved. Thus, the 85 kDa band
108 corresponds to the S2 segment (S_2) of the SARS-CoV-2 S, as the primary antibody recognizes the S2 region,
109 while the 185 kDa band corresponds to the uncleaved (S_0) SARS-CoV S. We note that the both SARS-CoVpp
110 and SARS-CoV-2pp exhibit bands at >185 kDa that likely corresponding to dimeric and trimeric forms of S.
111 These oligomeric forms of S have been reported in other SARS-CoV-2pp western blots[22,28]. Since SARS-
112 CoVpp harbor full-length S, their oligomeric S bands are of higher molecular weight than the SARS-CoV-
113 2pp oligomeric S bands, which harbor cleaved S. Furthermore, the higher order bands may be more
114 apparent due to the use of a polyclonal antibody to detect both the SARS-CoV and SARS-CoV-2 S.

115 **Figure 2**

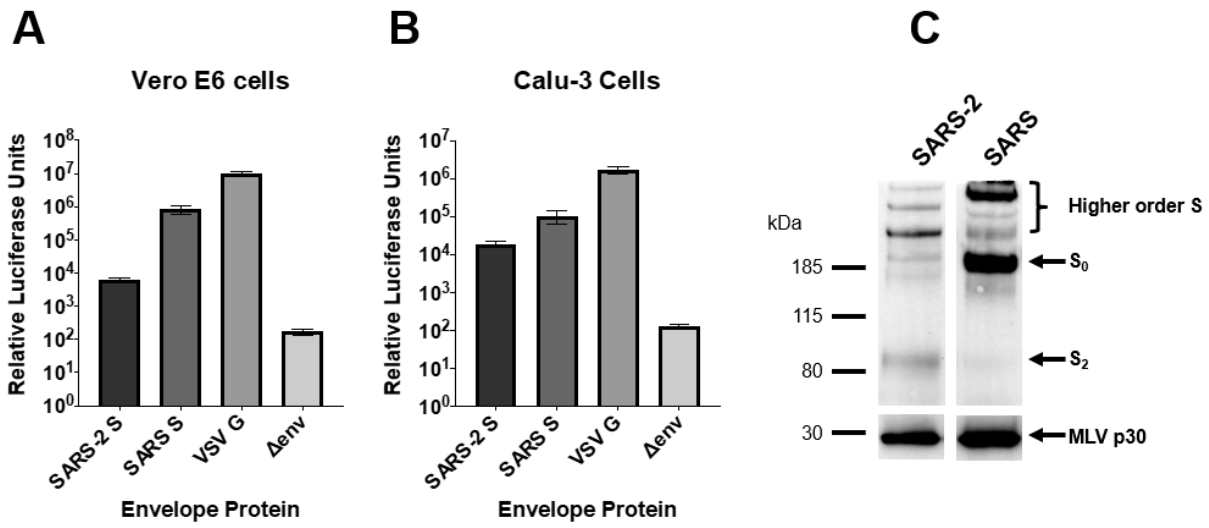

116

117 **Figure 2:** Characterization of MLVpp system. (**A and B**) MLVpp infectivity in Vero E6 and Calu-3 cells. Cells
118 were infected with MLVpps exhibiting the SARS-CoV-2 S, SARS-CoV S, VSV G or no envelope protein and
119 assessed for luciferase activity. Error bars represent the standard error measurements of three biological
120 replicates (n=3). (**C**) Western blot analysis of SARS-CoV-2pp and SARS-CoVpp S content. S was detected
121 using a rabbit antibody against the SARS-CoV-2 S2 region and cross reacts against the SARS-CoV S. MLV
122 content was detected using a mouse antibody against MLV p30. Image cropped from a singular western
123 blot.

124 **Use of the dec-RVKR-CMK protease inhibitor to produce SARS-2pp with uncleaved S.** To examine the
125 functional role of S priming by furin/PC proteases, we needed to produce SARS-CoV-2pp expressing
126 uncleaved S protein. This can be accomplished by treating producer cells with an appropriate protease
127 inhibitor to prevent S1/S2 cleavage during biogenesis. We chose dec-RVKR-CMK because it has been
128 shown to inhibit furin/PCs, preventing S1/S2 cleavage[23,26,29]. We have previously showed that addition of
129 dec-RVKR-CMK to producer cells generates MLV pseudotyped particles that harbor full-length MERS-CoV
130 S protein (MERS-CoVpp)[26] and we observe a similar trend with SARS-CoV-2pp generated from cells treated
131 with dec-RVKR-CMK (**Figure 3C,** lanes 1 and 2), exhibiting full-length uncleaved S_0 and weak cleaved S_2
132 bands. As mentioned, the additional bands at >185 kDa likely corresponding to dimeric and trimeric S, as
133 previously reported in other western blots probing for SARS-CoV-2pp S[22,28], with the higher order bands
134 from particles produced in cells treated with dec-RVKR-CMK observed at higher molecular weights.

135 The dec-RVKR-CMK-treated (uncleaved) particles were used to transduce cells to observe the impact of
136 S1/S2 cleavage for subsequent S2' activation via early acting TMPRSS2 in Calu-3 cells or late acting
137 cathepsin L in Vero E6 cells. In Vero E6 cells, the uncleaved SARS-CoV-2pp were 30-fold more infectious
138 than their cleaved counterparts, suggesting that uncleaved particles result in more infectious particles,
139 and that the S1/S2 pre-cleavage is not required or hinders infection via the late pathway (**Figure 3A**).
140 However, in Calu-3 cells, the opposite trend was observed; the uncleaved particles were significantly less
141 infectious than their cleaved counterparts (**Figure 3B**)**,** suggesting that S1/S2 pre-cleavage is essential[23,24]
142 for early entry. As a control, we also generated SARS-CoVpp, which lacks the furin/PC S1/S2 site, in the
143 presence or absence of dec-RVKR-CMK and noted no significant impact of dec-RVKR-CMK on SARS-CoVpp
144 infectivity in both Vero E6 and Calu-3 cells (**Figure S1A and S1B**). This affirms that the dec-RVKR-CMK
145 impacts on infectivity is due to blocking S1/S2 cleavage.

146 Thus, we were interested to see if we could restore the infection of the uncleaved particles by treating
147 them with exogeneous furin, which has been previously shown to process purified SARS-CoV-2 S protein[30].
148 In Calu-3, we observed a 2-fold increase in infection when uncleaved particles were treated with
149 exogeneous furin, but with cleaved particles, we did not observe any statistically significant increase with
150 furin treatment (**Figure 3B**). In Vero E6 cells, for both types of particles, we did not observe a statistically
151 significant increase in infection with furin treatment. (**Figure 3A**).

152 Since furin treatment only modestly increased infectivity in all cases observed, we wanted to visualize
153 how efficiently furin was processing the SARS-CoV-2 S via western blot. For cleaved particles, exogeneous
154 furin processed the faint full-length S_0 band into S_2 (**Figure 3C**, lanes 1 and 3). This trend was confirmed
155 upon quantifying the intensities of the S_0 and S_2 bands relative to the intensity of the MLV p30 band; furin
156 treatment reduced the relative S_0 intensity from 0.35 to 0.02, resulting in an increase in relative S_2
157 intensity from 1.74 to 2.83. For uncleaved particles, furin treatment had a more modest impact, as the
158 relative intensity of the S_0 bands was reduced from 2.61 to 2.25, resulting in a small increase in relative S_2
159 intensity from 0.66 to 0.92 (**Figure 3C**, lanes 2 and 4).

160 The western blot bands also reveal that the relative intensity of the uncleaved SARS-CoV-2pp S_0 bands are
161 greater than the relative intensity of the cleaved SARS-CoV-2pp S_2 bands and this trend was previously
162 observed with MERS-CoVpp S[26] (**Figure 3C**, lanes 1 and 2), but not with SARS-CoV (**Figure S1C**). This likely
163 suggests that the increased infectivity we observed with the uncleaved SARS-CoV-2pp in Vero E6 cells
164 could be due to particles harboring a greater amount of S protein. A possible explanation why uncleaved
165 particles could harbor more S is because uncleaved S is more stable than cleaved S, as S1/S2 cleavage
166 reduces S stability[30]. Thus, cleavage may encourage greater S degradation, reducing the amount of S
167 available for incorporation into pseudoparticles. However, we did not observe increased infectivity with

168 uncleaved SARS-CoV-2pp in Calu-3 cells because of the S1/S2 cleavage requirement and increased S

169 content cannot compensate for cleavage.

170 **Figure 3**

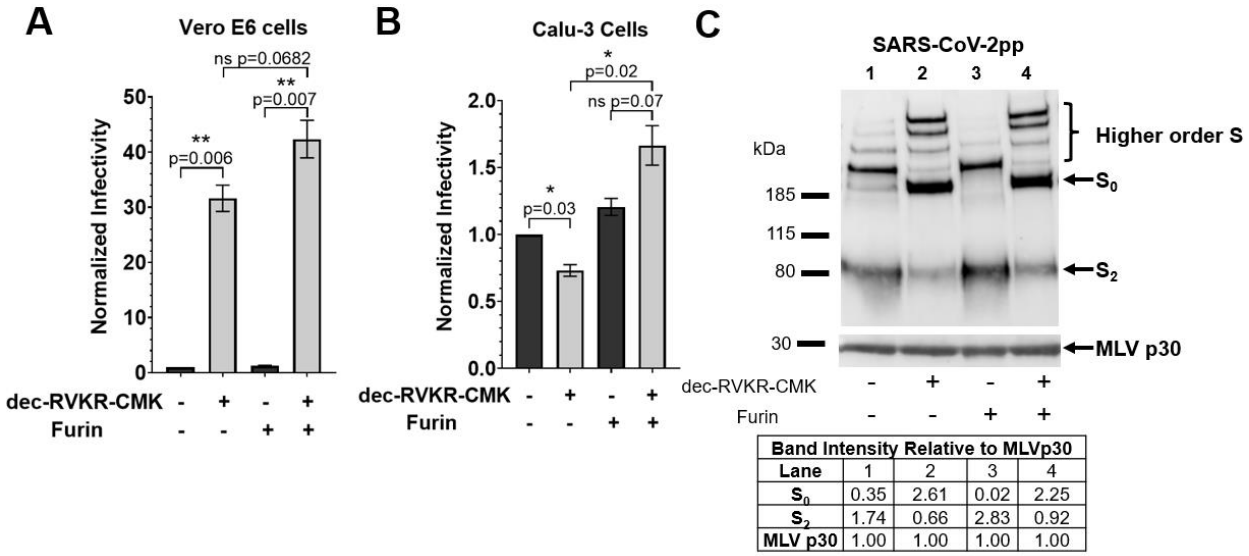

Band Intensity Relative to MLVp30				
Lane	1	2	3	4
S_0	0.35	2.61	0.02	2.25
S_2	1.74	0.66	2.83	0.92
MLV p30	1.00	1.00	1.00	1.00

171

172 **Figure 3**: Impact of dec-RVKR-CMK on MLVpps. + dec-RVKR-CMK refers to MLVpp produced in HEK293T
173 treated with 75 µM of dec-RVKR-CMK at the time of transfection. + Furin refers to particles treated with
174 6 U of recombinant furin for 3 hours at 37°C. (**A and B**) +/- dec-RVKR-CMK and +/- Furin SARS-CoV-2pp
175 were used to infect Vero E6 and Calu-3 cells. Infectivity was normalized to the – dec-RVKR-CMK – furin
176 condition in each cell line. Note the change in y-axis scale between A and B. Error bars represent the
177 standard error measurements of three biological replicates (n=3). Statistical analysis was performed using
178 an unpaired student's t test. Not shown: there is a ns difference between the – dec-RVKR-CMK +/- furin
179 conditions (black bars). *, $P \leq 0.05$, **, $P \leq 0.01$, ns, non-significant, $P > 0.05$. (**C**) Western blot analysis of
180 SARS-CoV-2pp produced in +/- dec-RVKR-CMK and treated with +/- furin for S protein content to
181 complement the infection conditions. S was detected using a rabbit antibody against the SARS-CoV-2 S2
182 region. MLV content was detected using a mouse antibody against MLV p30. Band intensities were
183 normalized to the MLV p30 band intensity.

184 Due to the limited ability of exogenous furin to rescue and cleave SARS-CoV-2 S, we re-evaluated the role
185 of furin in processing the S1/S2 site. Since dec-RVKR-CMK can also inhibit a number of furin related PCs,
186 the effects that have been observed with dec-RVKR-CMK on particles could have resulted from inhibition
187 of other PC proteases and not necessarily furin. Therefore, we produced particles in the presence of
188 alpha1-PDX, a more selective furin inhibitor[31] than dec-RVKR-CMK. Infectivity results of these particles in
189 Vero E6 cells show that the alpha1-PDX furin specific inhibitor failed to recapitulate the high level of
190 enhancement provided by dec-RVKR-CMK at all tested inhibitor concentrations (**Figure 4A**). This indicates
191 that dec-RVKR-CMK may have also been acting on non-furin proteases that can also process the S1/S2 site
192 and furin itself may not be the only protease processing the S1/S2 site, as is generally assumed.

193 As a control, the activity of the alpha1-PDX was confirmed using a proteolytic cleavage assay, in which
194 proteolytic cleavage of fluorogenic peptides results in a fluorescence increase used to determine the
195 velocity of the cleavage reaction (Vmax). We have previously used this assay to observe furin cleavage of
196 fluorogenic peptides mimicking the SARS-CoV-2 S1/S2 site (TNSPRRARSVA)[32]. Addition of the alpha1-PDX
197 or dec-RVKR-CMK inhibitor to a peptide reaction including furin resulted in almost complete inhibition of
198 activity, as very limited cleavage was detected. Interestingly, addition of the alpha1-PDX or dec-RVKR-
199 CMK to a reaction including trypsin gave different results. While alpha1-PDX did modestly inhibited
200 trypsin-mediated cleavage, dec-RVKR-CMK exhibited almost complete inhibition of trypsin activity. Thus,
201 the results of this peptide cleavage assay confirm that alpha1-PDX is active on furin-like substrates and is
202 a much more specific inhibitor compared to dec-RVKR-CMK (**Figure 4B**).

203 Our published results demonstrated that the PC protease PC1 can process SARS-CoV-2 S1/S2[32], which
204 opens up the possibility that non-furin proteases within the secretory pathway in producer cells can
205 process the SARS-CoV-2 “furin-like” S1/S2 site, as originally suggested by Coutard et al[33]. In the studies
206 reported here, we utilize HEK293T cells to produce the pseudoparticles, which may express a different

207 repertoire of proteases than those in clinically relevant cells. In the future, it will be important to

208 investigate the impact of S1/S2 processing by non-furin PCs in cells infected with SARS-CoV-2.

209 **Figure 4**

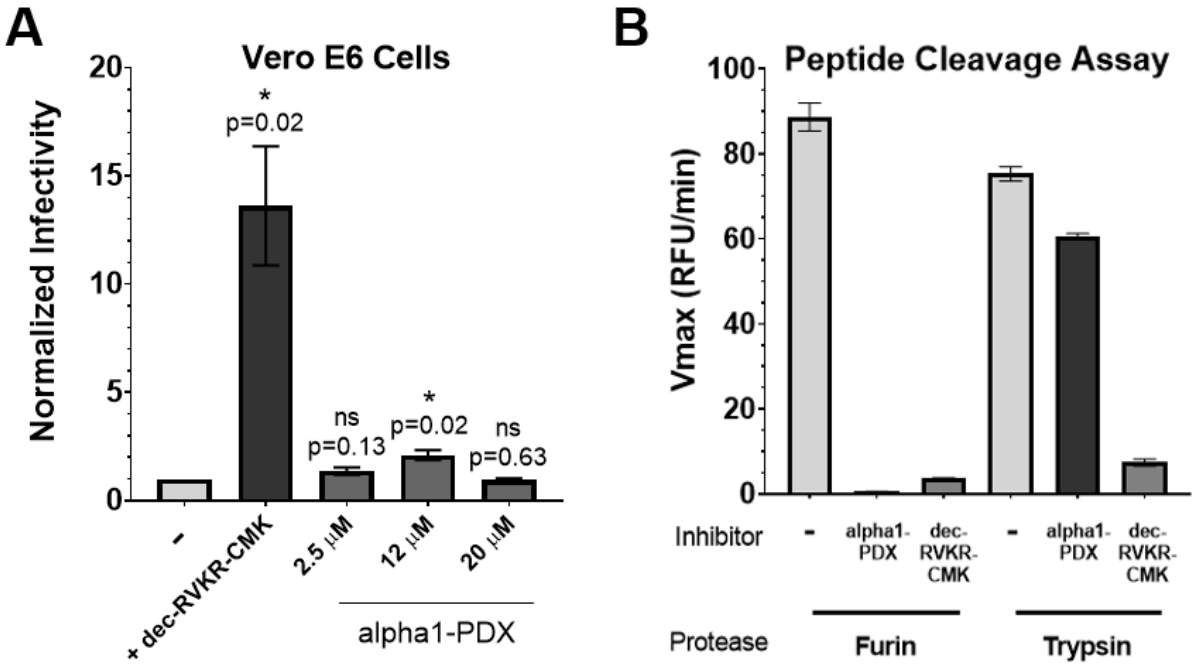

210

211 **Figure 4**: Use of specific furin (alpha1-PDX) and broad furin (dec-RVKR-CMK) inhibitors to investigate furin
212 specificity. **(A)** Infectivity of particles produced in the presence of broad (dec-RVKR-CMK) and specific
213 (alpha1-PDX) furin inhibitors. Inhibitor was applied at the indicated concentration to producer HEK293T
214 cells. Particles were used to infect Vero E6 cells. Infectivity was normalized to the – condition. Error bars
215 represent the standard error measurements of four biological replicates (n=4). Statistical analysis was
216 performed using an unpaired student's t test compared to - condition. *, P ≤0.05, ns, non-significant, P >
217 0.05. **(B)** Proteolytic cleavage assay of SARS-CoV-2 S1/S2 peptides to confirm alpha1-PDX and dec-RVKR-
218 CMK inhibition specificity. Alpha1-PDX (2 µM), dec-RVKR-CMK (75 µM) or no inhibitor was incubated with
219 either furin or trypsin recombinant protease and a fluorogenic peptides mimicking the SARS-CoV-2 S1/S2
220 site (TNSPRRARSVA). Results represent averages and error bars represent the standard error
221 measurement of three biological replicates (n=3).

222 **Furin-cleavage predictions of the SARS-CoV-2 S1/S2 site.** To gain further insights on furin processing of
223 the S1/S2 sites, we utilized the PiTou[34] and ProP[35] cleavage prediction tools to analyze the likelihood that
224 the S1/S2 site is processed by furin. ProP predicts furin cleavage sites based on networks derived from
225 experimental data, whereas PiTou uses a combination of a hidden Markov model and biological
226 knowledge-based cumulative probability score functions to characterize a 20 amino acid motif from P14
227 to P6' that reflects the binding strength and accessibility of the motif in the furin binding pocket. Thus,
228 the PiTou algorithm has been reported to be more sensitive and specific than ProP for predicting furin
229 cleavage[34]. Both algorithms agree with each other in predicting furin cleavage, with positive scores (PiTou)
230 and scores above 0.5 (ProP) indicating furin cleavage, strengthening the predictions (**Figure 5**), but since
231 the PiTou algorithm is more sensitive and specific, we decided to focus on the PiTou values for further
232 analysis.

233 The PiTou algorithm predicts that the SARS-CoV-2 S1/S2 site (PiTou score: 9.2) can be cleaved by furin,
234 whereas other lineage B CoVs that have been proposed as SARS-CoV-2 precursors, such as SARS-CoV,
235 RaTG13, ZC45, ZXC21 and RmYN02, are predicted not to be cleaved by furin. Notably, the PiTou scores of
236 traditionally accepted furin cleavage sites, such as those found in influenza H5N1 (PiTou score: 13.6) and
237 HCoV-HKU1 (PiTou score: 14.6), are much higher than for SARS-CoV-2, suggesting that while SARS-CoV-2
238 S1/S2 site has increased furin recognition when compared to other lineage B-betaCoVs, the site is not
239 optimal for furin cleavage, in alignment with the experimental data shown here suggesting poor furin
240 specific cleavage.

241 The modest SARS-CoV-2 PiTou score raises question about the origin and evolution of the S1/S2 site of
242 the virus. It is generally believed that the SARS-CoV-2 S1/S2 site is an insertion of "polybasic" residues[36],
243 as occurs for avian influenza virus, but as the identity of the SARS-CoV-2 ancestor virus still remains to be
244 discovered, it is important to explore alternative explanations. It has recently been proposed that

245 unsampled SARS-like CoV lineages(s) may be circulating in bats, which are important for the evolutionary
246 origins of SARS-CoV-2[37]. Of note, a "breakpoint sequence hypothesis" has been proposed for the
247 introduction of a furin-like cleavage site at S1/S2[38], an idea further elucidated by Lytras et al[39] in the
248 context of the origin of SARS-like viruses. We consider that SARS-CoV-2 could have originated via
249 recombination with a currently unknown ancestor bat virus with a robust furin cleavage site (i.e. PiTou
250 score approx. 13-15), but one which cannot bind to a human receptor—and that in order to gain the ability
251 to infect human cells, the furin cleavage site may have been down-regulated.

252 These suggested parallels are informed by betaCoV lineage C in which MERS-CoV has a modest furin score
253 (PiTou score: 5.2), but its closest known ancestor bat viruses, BatCoV-HKU4 (PiTou score: <0), BatCoV-
254 HKU5 (PiTou score: 10.3), and BatCoV-PML (PiTou score: 2.175) exhibit a wide range of furin scores. Of
255 note is that the virus with the highest furin score, BatCoV-HKU5 (PiTou score: 10.3), cannot bind the MERS-
256 CoV hDPP4 receptor, whereas BatCoV-HKU4 (PiTou score: <0) can[40], so the MERS-CoV S1/S2 site can be
257 seen as a down-regulation from BatCoV-HKU5 to bind hDPP4.

258 **Figure 5**

	S1/S2 Sequence	Furin Score PiTou	Furin Score ProP
Betacoronavirus			
Lineage A			
HCoV-HKU1	747-YNSPSSSSSRRKRR|SISASY-766	**+14.634**	**0.918**
Lineage B			
SARS-CoV	654-AGICASYHTVSLLR|STSQKS-673	-5.167	0.123
SARS-CoV-2	672-ASYQTQTNSPRRAR|SVASQS-691	**+9.196**	**0.620**
Bat-RmYN02*	667-AGVCASYNSPAA-R|VGTNSI-686	-5.085	0.111
Bat-CoV RaTG13	668-AGICASYQTQTNSR|SVASQS-687	-4.672	0.151
Bat-CoV ZC45	645-AGICASYHTASILR|STSQKA-664	-5.333	0.153
Bat-CoV ZXC21	644-AGICASYHTASILR|STGQKA-663	-5.333	0.170
Lineage C			
MERS-CoV	738-LPDTPSTLTPRSVR|SVPGEM-757	**+5.155**	**0.563**
BatCoV-HKU4	736-GQSLCAVPPVSTFR|SYSASQ-755	-5.14	0.229
BatCoV-HKU5	732-LCAIPPTTSSRVRR|ATSGAS-751	**+10.259**	**0.822**
BatCoV-PML	732-LCAIPPNTNLRSGR|STFGLG-751	**+2.175**	**0.572**
Lineage D			
BatCoV-HKU9	663-NGSIATANADSLPR|LQLVNY-682	-4.767	0.064
Influenza A			
H5N1	322-LRNTPQRERRRKKR|GLFGAI-341	**+13.59**	**0.808**

259

260 **Figure 5.** Furin cleavage score analysis of CoV S1/S2 cleavage sites. CoV S sequences were analyzed using
261 the ProP[35] 1.0 and PiTou[34] 3.0 furin prediction algorithm. Bold scores indicate the S1/S2 sequence is
262 predicted to be cleaved by furin. Purple lines denote the position of the predicted S1/S2 cleavage site.
263 Basic arginine (R) and lysine (K) residues are highlighted in blue. *For Bat-RmYN02, sequence number was
264 determined from S alignment with SARS-CoV-2 S using Geneious. Sequences corresponding to the S1/S2
265 region of HCoV-HKU1 (AAT98580.1), SARS-CoV (AAT74874.1), SARS-CoV-2 (QHD43416.1), Bat-CoVRaTG13
266 (QHR63300.2), Bat-SL-CoVZC45 (AVP78031.1), Bat-SL-CoVZXC21 (AVP78042.1), MERS-CoV (AFS88936.1),
267 BatCoV-HKU4 (YP_001039953.1), BatCoV-HKU5 (YP_001039962.1), BatCoV-PML (KC869678), Bat-CoV-
268 HKU9 (YP_001039971), and Influenza A/Chicken/Hong Kong/822.1/01/H5N1 (AF509026.2) were obtained
269 from GenBank. Sequences corresponding to the S1/S2 region of RmYN02 (EPI_ISL_412977) was obtained
270 from GISAID.

271 Overall, our results support observations[23,24] that the role of this "gained" SARS-CoV-2 S1/S2 site is to
272 expand viral tropism to respiratory cells, likely in the upper airways, allowing efficient transmission.
273 Cleaved S1/S2 site is crucial for the SARS-CoV-2 S to be subsequently cleaved at the S2' location by
274 TMPRSS2 for early entry in respiratory cells. Without the S1/S2 pre-cleavage, we predict that SARS-CoV-2
275 would be endocytosed and due to low cathepsin L expression in respiratory endosomes[7], SARS-CoV-2
276 would not efficiently infect via this route. If SARS-CoV-2 infects TMPRSS2 negative cells, it can utilize
277 endosomal cathepsin L, an ubiquitous protease generally found throughout mammalian cells[41], to activate
278 the S protein[22]—though at undetermined sites. However, for cathepsin L activation, S1/S2 pre-cleavage is
279 not required, and our results indicate that preventing this cleavage increases infectivity of SARS-CoV-2, at
280 least in Vero E6 cells. This may be connected to recent work showing that S1/S2 pre-cleavage reduces the
281 thermal stability of SARS-CoV-2 S[30] and by preventing this cleavage, there is more S available for
282 incorporation into pseudoparticles. Interestingly, the S1/S2 site activation appears to also have a role in
283 the immune response against SARS-CoV-2, as it has been shown that SARS-CoV-2 S with a deleted S1/S2
284 loop can provide better protective immune response than with the S1/S2 loop[42].

285 The role of furin in activating the S1/S2 site was also investigated. As protease inhibitors commonly
286 employed in cell entry studies, such as dec-RVKR-CMK, can also inhibit other proteases in addition to
287 furin[29], it is difficult to ascertain the impact of individual proteases. While furin likely processes the SARS-
288 CoV-2 site, our data suggests that other PCs are also involved, since western blots show poor processing
289 of uncleaved S upon addition of purified furin and the use of a highly selective furin inhibitor (alpha1-PDX)
290 has a modest impact on infectivity. All in all, as we consider protease-based inhibitors in treating COVID-
291 19, especially those targeting furin[43,44], it is important to thoroughly evaluate the role of these proteases
292 to be certain that the relevant proteases are targeted.

293 **Methods**

294 **Predicted structural modeling.** S protein models were built using UCSF Chimera (v.1.14, University of
295 California) through modeler homology tool of the Modeller extension (v.9.25, University of California) as
296 described[15]. SARS-CoV and SARS-CoV-2 S models were built based on the SARS-CoV S structure (PDB No.
297 5X58).

298 **Cells, plasmids, and reagents**. HEK293T (accession no: CRL-11268, ATCC), Vero E6 (accession no: CRL-1586,
299 ATCC), and Calu-3 (accession no: HTB-55) cells were maintained at 37°C and 5% CO_2 incubator and
300 cultivated in Dulbecco's Modified Eagle Medium (Cellgro) supplemented with 10% Hyclone FetalClone II
301 (GE) and 10 mM HEPES (Cellgro) (DMEMc). Cells were passaged using Dulbecco's Phosphate-Buffered
302 Saline (DPBS) and Trypsin EDTA 1x (Cellgro). The pCMV-MLV-gagpol murine leukemia virus (MLV)
303 packaging construct, the pTG-luc luciferase reporter, pCAGGS/VSV-G, pCAGGS, and pcDNA/SARS-S
304 plasmids are as previously described[25]. The pcDNA/SARS2-S was a generous gift from Veesler lab[21].

305 Protease inhibitor decanoyl-RVKR-CMK (dec-RVKR-CMK) was purchased from Tocris and resuspended in
306 sterile water to 10 mM. Recombinant furin was purchased from New England Biolabs. Recombinant L-1-
307 Tosylamide-2-phenylethyl chloromethyl ketone (TPCK)-treated trypsin was obtained from Sigma-Aldrich.
308 Human alpha-1 PDX (alpha1-PDX) recombinant protein was purchased from ThermoFisher Scientific.

309 The SARS-CoV-2 S1/S2 fluorogenic peptide with the sequence TNSPRRARSVA, sandwiched between the
310 (7-methoxycoumarin-4-yl)acetyl/2,4-dinitrophenyl (MCA/DNP) FRET pair, was synthesized by Biomatik.

311 **Furin prediction calculations.** Prop: CoV sequences were inputted into the ProP 1.0 Server hosted here:
312 cbs.dtu.dk/services/ProP/ PiTou: CoV sequences were analyzed using the PiTou V3 software freely
313 available via request here[34].

314 **Pseudoparticle production**. Pseudotyped virus were produced from published protocols with minor
315 modifications[25]. Briefly, HEK293T cells were seeded to 30% confluency. Cells were transfected with pTG-
316 luc (600 ng), pCMV-MLV-gagpol (800 ng), and the respective viral envelope protein (600 ng) using
317 polyethylenimine for 48 hours. Supernatants were then harvested, centrifuged, clarified, and stored in -
318 80°C aliquots.

319 For + dec-RVKR-CMK particles, 7.5 µL of dec-RVKR-CMK was added to cells immediately after transfection
320 and boosted with an additional 7.5 µL 24 hours later (final concentration: 75 µM).

321 For alpha1-PDX particles, indicated concentrations were added to cells immediately after transfection, as
322 recommended by the manufacturer.

323 **Pseudoparticle assays**. Infection assays were as previously described with minor modifications[25] in
324 triplicate. Briefly, target cells were seeded to confluency. Cells were washed with DPBS, infected with
325 particles on a rocker in an incubator with rocker for 1.5 hours. Cells were supplemented with DMEMc and
326 incubated for 72 hours. Cells were lysed and luciferase activity was assessed using the Luciferase Assay
327 System and the Glomax 20/20 luminometer (Promega). Infectivity values were analyzed and plotted using
328 Prism 8.

329 **Exogeneous protease treatment**. 1 mL pseudoparticles were pelleted using a TLA-55 rotor with an
330 Optima-MAX-E ultracentrifuge (Beckman Coulter) for 2 hours at 42,000 rpm at 4°C. Particles were
331 resuspended in 30 µL DPBS buffer supplemented with 20 mM HEPES, 0.2 mM CaCl2, 0.2 mM β-
332 mercaptoethanol (at pH 7.0). Particles were treated with 6 U recombinant furin for 3 hours at 37°C.

333 **Western blot analysis of pseudoparticles**. 3 mL pseudoparticles were pelleted and resuspended as
334 described above, but in 20 µL. Sodium dodecyl sulfate (SDS) loading buffer and DTT were added to samples
335 and heated at 65°C for 20 minutes. Samples were separated on NuPAGE Bis-Tris gel (Invitrogen) and

336 transferred on polyvinylidene difluoride membranes (GE). SARS-CoV-2 and SARS-CoV S was detected using
337 a rabbit polyclonal antibody that recognizes the S2 domain (Cat: 40590-T62, Sinobiological) and an
338 AlexaFluor 488 goat anti-rabbit secondary antibody. MLV protein was detected using a mouse monoclonal
339 antibody that recognizes the MLV p30 protein (Cat: ab130757, abcam) and an AlexaFluor 488 goat anti-
340 mouse secondary antibody. Bands were detected using the ChemiDoc Imaging software (Bio-Rad). S_0 and
341 S_2 band intensity was calculated using the analysis tools on Biorad Image Lab 6.1 software and normalized
342 to the MLV p30 band intensity.

343 **Fluorogenic peptide assay**. Peptide assays were as previously described with minor modifications[32] in
344 triplicates. Each reaction was performed in a 100 µL volume consisting of buffer, protease, inhibitor, and
345 SARS-CoV-2 S1/S2 fluorogenic peptide in an opaque 96-well plate. For furin catalyzed reactions, 1 U/well
346 recombinant furin was diluted in buffer consisting of 20 mM HEPES, 0.2 mM $CaCl_2$, 0.2 mM β-
347 mercaptoethanol. For trypsin catalyzed reactions, 0.8 nM/well TPCK trypsin was diluted in PBS buffer. The
348 alpha1-PDX inhibitor or dec-RVKR-CMK inhibitor were added at a concentration of 2 µM or 75 µM,
349 respectively. Peptide was lastly added at a concentration of 50 µM.

350 Fluorescence emission was measured every minute for 60 minutes using a SpectraMax fluorometer
351 (Molecular Devices) at 30°C using an excitation wavelength of 330 nm and an emission wavelength of 390
352 n. Vmax was calculated by fitting the linear rise in fluorescence to the equation of a line.

353 **Acknowledgments**

354 This work was funded by the National Institute of Health research grant R01AI35270 and Fast Grant,
355 Mercatus Center. TT acknowledges support by the National Science Foundation Graduate Research
356 Fellowship Program under Grant No. DGE-1650441 and the Samuel C. Fleming Family Graduate Fellowship.
357 We would especially like to thank Jean Millet for providing important insight on analyzing PiTou values
358 and calculations for BatCoV-HKU9. We would like to thank Hector Aguilar-Carreno for helpful input and

359 thank members of the Daniel and Whittaker groups as well as the Eliezer and Weinstein groups at Weill
360 Cornell for helpful discussions. SD acknowledges funding for this project, sponsored by the Defense
361 Advanced Research Projects Agency (DARPA) Army Research Office and accomplished under Cooperative
362 Agreement Number W911NF-18-2-0152. The views and conclusions contained in this document are those
363 of the authors and should not be interpreted as representing the official policies, either expressed or
364 implied, of DARPA or the Army Research Office or the U.S. Government. The U.S. Government is
365 authorized to reproduce and distribute reprints for Government purposes notwithstanding any copyright
366 notation herein.

367

368 **Supporting Information**

369 Supporting information available: Impact of dec-RVKR-CMK inhibitor on SARS-CoVpp production, which
370 lacks the furin S1/S2 site (**Figure S1**).

371

372

373 **References**

374 1. Zhong, N. S., Zheng, B. J., Li, Y. M., Poon, L. L. M., Xie, Z. H., Chan, K. H., Li, P. H., Tan, S. Y., Chang,
375 Q., Xie, J. P., Liu, X. Q., Xu, J., Li, D. X., Yuen, K. Y., Peiris, J. S. M., Guan, Y. Epidemiology and cause
376 of severe acute respiratory syndrome (SARS) in Guangdong, People's Republic of China, in
377 February, 2003. *Lancet* **362**, 1353–1358 (2003).

378 2. Zaki, A. M., van Boheemen, S., Bestebroer, T. M., Osterhaus, A. D. M. E., Fouchier, R. A. M.
379 Isolation of a Novel Coronavirus from a Man with Pneumonia in Saudi Arabia. *N. Engl. J. Med.*
380 **367**, 1814–1820 (2012).

381 3. Zhu, N., Zhang, D., Wang, W., Li, X., Yang, B., Song, J., Zhao, X., Huang, B., Shi, W., Lu, R., Niu, P.,
382 Zhan, F., Ma, X., Wang, D., Xu, W., Wu, G., Gao, G. F., Tan, W. A novel coronavirus from patients
383 with pneumonia in China, 2019. *N. Engl. J. Med.* **382**, 727–733 (2020).

384 4. Belouzard, S., Millet, J. K., Licitra, B. N., Whittaker, G. R. Mechanisms of coronavirus cell entry
385 mediated by the viral spike protein. *Viruses* **4**, 1011–1033 (2012).

386 5. White, J. M., Whittaker, G. R. Fusion of Enveloped Viruses in Endosomes. *Traffic* **17**, 593–614
387 (2016).

388 6. Heald-Sargent, T., Gallagher, T. Ready, Set, Fuse! The Coronavirus Spike Protein and Acquisition
389 of Fusion Competence. *Viruses* **4**, 557–580 (2012).

390 7. Park, J. E., Li, K., Barlan, A., Fehr, A. R., Perlman, S., McCray, P. B., Gallagher, T. Proteolytic
391 processing of middle east respiratory syndrome coronavirus spikes expands virus tropism. *Proc.*
392 *Natl. Acad. Sci. U. S. A.* **113**, 12262–12267 (2016).

393 8. Shulla, A., Heald-Sargent, T., Subramanya, G., Zhao, J., Perlman, S., Gallagher, T. A
394 Transmembrane Serine Protease Is Linked to the Severe Acute Respiratory Syndrome
395 Coronavirus Receptor and Activates Virus Entry Downloaded from. *J. Virol.* **85**, 873–882 (2011).

396 9. Matsuyama, S., Nagata, N., Shirato, K., Kawase, M., Takeda, M., Taguchi, F. Efficient Activation of
397 the Severe Acute Respiratory Syndrome Coronavirus Spike Protein by the Transmembrane
398 Protease TMPRSS2. *J. Virol.* **84**, 12658–12664 (2010).

399 10. Glowacka, I., Bertram, S., Müller, M. A., Allen, P., Soilleux, E., Pfefferle, S., Steffen, I., Tsegaye, T.
400 S., He, Y., Gnirss, K., Niemeyer, D., Schneider, H., Drosten, C., Pöhlmann, S. Evidence that
401 TMPRSS2 Activates the Severe Acute Respiratory Syndrome Coronavirus Spike Protein for
402 Membrane Fusion and Reduces Viral Control by the Humoral Immune Response. *J. Virol.* **85**,
403 4122–4134 (2011).

404 11. Simmons, G., Gosalia, D. N., Rennekamp, A. J., Reeves, J. D., Diamond, S. L., Bates, P. *Inhibitors of*
405 *cathepsin L prevent severe acute respiratory syndrome coronavirus entry*. *Proceedings of the*
406 *National Academy of Sciences of the United States of America* vol. 102
407 www.pnas.orgcgidoi10.1073pnas.0505577102 (2005).

408 12. Millet, J. K., Whittaker, G. R. Host cell entry of Middle East respiratory syndrome coronavirus
409 after two-step, furin-mediated activation of the spike protein. *Proc. Natl. Acad. Sci. U. S. A.* **111**,
410 15214–15219 (2014).

411 13. Reinke, L. M., Spiegel, M., Plegge, T., Hartleib, A., Nehlmeier, I., Gierer, S., Hoffmann, M.,
412 Hofmann-Winkler, H., Winkler, M., Pöhlmann, S. Different residues in the SARS-CoV spike protein
413 determine cleavage and activation by the host cell protease TMPRSS2. *PLoS One* **12**(6):e0179177,
414 (2017).

415 14. Wrapp, D., Wang, N., Corbett, K. S., Goldsmith, J. A., Hsieh, C.-L., Abiona, O., Graham, B. S.,
416 McLellan, J. S. Cryo-EM structure of the 2019-nCoV spike in the prefusion conformation. *Science*
417 **367**, 1260–1263 (2020).

418 15. Jaimes, J. A., André, N. M., Chappie, J. S., Millet, J. K., Whittaker, G. R. Phylogenetic Analysis and

419 Structural Modeling of SARS-CoV-2 Spike Protein Reveals an Evolutionary Distinct and
420 Proteolytically Sensitive Activation Loop. *J. Mol. Biol.* **432**, 3309–3325 (2020).

421 16. Henrich, S., Lindberg, I., Bode, W., Than, M. E. Proprotein convertase models based on the crystal
422 structures of furin and kexin: Explanation of their specificity. *J. Mol. Biol.* **345**, 211–227 (2005).

423 17. Henrich, S., Cameron, A., Bourenkov, G. P., Kiefersauer, R., Huber, R., Lindberg, I., Bode, W.,
424 Than, M. E. The crystal structure of the proprotein processing proteinase furin explains its
425 stringent specificity. *Nat. Struct. Biol.* **10**, 520–526 (2003).

426 18. Tian, S., Huang, Q., Fang, Y., Wu, J. FurinDB: A Database of 20-residue furin cleavage site motifs,
427 substrates and their associated drugs. *Int. J. Mol. Sci.* **12**, 1060–1065 (2011).

428 19. Abrami, L., Fivaz, M., Decroly, E., Seidah, N. G., Jean, F., Thomas, G., Leppla, S. H., Buckley, J. T.,
429 Van Der Goot, F. G. The pore-forming toxin proaerolysin is activated by furin. *J. Biol. Chem.* **273**,
430 32656–32661 (1998).

431 20. Hoffmann, M., Kleine-Weber, H., Schroeder, S., Krüger, N., Herrler, T., Erichsen, S., Schiergens, T.
432 S., Herrler, G., Wu, N. H., Nitsche, A., Müller, M. A., Drosten, C., Pöhlmann, S. SARS-CoV-2 Cell
433 Entry Depends on ACE2 and TMPRSS2 and Is Blocked by a Clinically Proven Protease Inhibitor.
434 *Cell* **181**, 271-280.e8 (2020).

435 21. Walls, A. C., Park, Y.-J., Tortorici, M. A., Wall, A., McGuire, A. T., Veesler, D. Structure, Function,
436 and Antigenicity of the SARS-CoV-2 Spike Glycoprotein. *Cell* (2020)
437 doi:10.1016/j.cell.2020.02.058.

438 22. Ou, X., Liu, Y., Lei, X., Li, P., Mi, D., Ren, L., Guo, L., Guo, R., Chen, T., Hu, J., Xiang, Z., Mu, Z., Chen,
439 X., Chen, J., Hu, K., Jin, Q., Wang, J., Qian, Z. Characterization of spike glycoprotein of SARS-CoV-2
440 on virus entry and its immune cross-reactivity with SARS-CoV. *Nat. Commun.* **11**, 1620 (2020).

441 23. Hoffmann, M., Kleine-Weber, H., Pöhlmann, S. A Multibasic Cleavage Site in the Spike Protein of

442 SARS-CoV-2 Is Essential for Infection of Human Lung Cells. *Mol. Cell* **78**, 779-784.e5 (2020).

443 24. Bestle, D., Heindl, M. R., Limburg, H., Van Lam van, T., Pilgram, O., Moulton, H., Stein, D. A.,
444 Hardes, K., Eickmann, M., Dolnik, O., Rohde, C., Klenk, H. D., Garten, W., Steinmetzer, T.,
445 Böttcher-Friebertshäuser, E. TMPRSS2 and furin are both essential for proteolytic activation of
446 SARS-CoV-2 in human airway cells. *Life Sci. alliance* **3**, (2020).

447 25. Millet, J. K., Tang, T., Nathan, L., Jaimes, J. A., Hsu, H. L., Daniel, S., Whittaker, G. R. Production of
448 pseudotyped particles to study highly pathogenic coronaviruses in a biosafety level 2 setting. *J.*
449 *Vis. Exp.* **2019**, e59010 (2019).

450 26. Straus, M. R., Tang, T., Lai, A. L., Flegel, A., Bidon, M., Freed, J. H., Daniel, S., Whittaker, G. R. Ca
451 2+ ions promote fusion of Middle East respiratory syndrome coronavirus with host cells and
452 increase infectivity . *J. Virol.* **94**, 426–446 (2020).

453 27. Tang, T., Bidon, M., Jaimes, J. A., Whittaker, G. R., Daniel, S. Coronavirus membrane fusion
454 mechanism offers a potential target for antiviral development. *Antiviral Res.* **178**, 104792 (2020).

455 28. Hyseni, I., Molesti, E., Benincasa, L., Piu, P., Casa, E., Temperton, N. J., Manenti, A., Montomoli, E.
456 Characterisation of SARS-CoV-2 Lentiviral Pseudotypes and Correlation between Pseudotype-
457 Based Neutralisation Assays and Live Virus-Based Micro Neutralisation Assays. *Viruses* **12**, 1011
458 (2020).

459 29. Matsuyama, S., Shirato, K., Kawase, M., Terada, Y., Kawachi, K., Fukushi, S., Kamitani, W. Middle
460 East Respiratory Syndrome Coronavirus Spike Protein Is Not Activated Directly by Cellular Furin
461 during Viral Entry into Target Cells. *J. Virol.* **92**, (2018).

462 30. Wrobel, A. G., Benton, D. J., Xu, P., Roustan, C., Martin, S. R., Rosenthal, P. B., Skehel, J. J.,
463 Gamblin, S. J. SARS-CoV-2 and bat RaTG13 spike glycoprotein structures inform on virus evolution
464 and furin-cleavage effects. *Nat. Struct. Mol. Biol.* **27**, 763–767 (2020).

465 31. Jean, F., Stella, K., Thomas, L., Liu, G., Xiang, Y., Reason, A. J., Thomas, G. α1-Antitrypsin Portland,
466 a bioengineered serpin highly selective for furin: Application as an antipathogenic agent. *Proc.*
467 *Natl. Acad. Sci. U. S. A.* **95**, 7293–7298 (1998).

468 32. Jaimes, J. A., Millet, J. K., Whittaker, G. R. Proteolytic Cleavage of the SARS-CoV-2 Spike Protein
469 and the Role of the Novel S1/S2 Site. *iScience* **23**, (2020).

470 33. Coutard, B., Valle, C., de Lamballerie, X., Canard, B., Seidah, N. G., Decroly, E. The spike
471 glycoprotein of the new coronavirus 2019-nCoV contains a furin-like cleavage site absent in CoV
472 of the same clade. *Antiviral Res.* **176**, 104742 (2020).

473 34. Tian, S., Huajun, W., Wu, J. Computational prediction of furin cleavage sites by a hybrid method
474 and understanding mechanism underlying diseases. *Sci. Rep.* **2**, (2012).

475 35. Duckert, P., Brunak, S., Blom, N. Prediction of proprotein convertase cleavage sites. *Protein Eng.*
476 *Des. Sel.* **17**, 107–112 (2004).

477 36. Andersen, K. G., Rambaut, A., Lipkin, W. I., Holmes, E. C., Garry, R. F. The proximal origin of SARS-
478 CoV-2. *Nat. Med.* **89**, 44–48 (2020).

479 37. Boni, M. F., Lemey, P., Jiang, X., Lam, T. T. Y., Perry, B. W., Castoe, T. A., Rambaut, A., Robertson,
480 D. L. Evolutionary origins of the SARS-CoV-2 sarbecovirus lineage responsible for the COVID-19
481 pandemic. *Nat. Microbiol.* **5**, 1408–1417 (2020).

482 38. Gallaher, W. R. A palindromic RNA sequence as a common breakpoint contributor to copy-choice
483 recombination in SARS-COV-2. *Arch. Virol.* **165**, 2341–2348 (2020).

484 39. Lytras, S., MacLean, O. A., Robertson, D. L. The Sarbecovirus origin of SARS-CoV-2's furin cleavage
485 site. *Virological* https://virological.org/t/the-sarbecovirus-origin-of-sars-cov-2-s-furin-cleavage-
486 site/536 (2020).

487 40. Yang, Y., Du, L., Liu, C., Wang, L., Ma, C., Tang, J., Baric, R. S., Jiang, S., Li, F. Receptor usage and

488 cell entry of bat coronavirus HKU4 provide insight into bat-to-human transmission of MERS
489 coronavirus. *Proc. Natl. Acad. Sci. U. S. A.* **111**, 12516–12521 (2014).

490 41. Mcgrath, M. E. *THE LYSOSOMAL CYSTEINE PROTEASES*. *Annu. Rev. Biophys. Biomol. Struct* vol. 28
491 www.annualreviews.org (1999).

492 42. Laczkó, D., Hogan, M. J., Toulmin, S. A., Hicks, P., Lederer, K., Gaudette, B. T., Castraño D.,
493 Amanat, F., Muramatsu, H., Oguin, T. H., Ojha, A., Zhang, L., Mu, Z., Parks, R., Manzoni, T. B.,
494 Roper, B., Strohmeier, S., Tombácz, I., Arwood, L., Nachbagauer, R., Karikó, K., Greenhouse, J.,
495 Pessaint, L., Porto, M., Putman-Taylor, T., Strasbaugh, A., Campbell, T. A., Lin, P. J., Tam, Y. K.,
496 Sempowski, G. D., Farzan, M., Choe, H., Saunders, K. O., Haynes, B. F., Andersen, H., Eisenlohr, L.
497 C., Weissman, D., Krammer, F., Bates, P., Allman, D., Locci, M., Pardi, N. A Single Immunization
498 with Nucleoside-Modified mRNA Vaccines Elicits Strong Cellular and Humoral Immune Responses
499 against SARS-CoV-2 in Mice. *Immunity* **53**, 724-732.e7 (2020).

500 43. Cheng, Y.-W., Chao, T.-L., Li, C.-L., Chiu, M.-F., Kao, H.-C., Wang, S.-H., Pang, Y.-H., Lin, C.-H., Tsai,
501 Y.-M., Lee, W.-H., Tao, M.-H., Ho, T.-C., Wu, P.-Y., Jang, L.-T., Chen, P.-J., Chang, S.-Y., Yeh, S.-H.
502 Furin Inhibitors Block SARS-CoV-2 Spike Protein Cleavage to Suppress Virus Production and
503 Cytopathic Effects. *Cell Rep.* **0**, 108254 (2020).

504 44. Edridge, A. W. D., Kaczorowska, J., Hoste, A. C. R., Bakker, M., Klein, M., Loens, K., Jebbink, M. F.,
505 Matser, A., Kinsella, C. M., Rueda, P., Ieven, M., Goossens, H., Prins, M., Sastre, P., Deijs, M., van
506 der Hoek, L. Seasonal coronavirus protective immunity is short-lasting. *Nat. Med.* **26**, (2020).